Unitary analytic isobar model for the reaction nucleon-meson to nucleon-meson-meson

I. J. R. Aitchison
Department of Theoretical Physics, University of Oxford, 1 Keble Road, Oxford OX1 3PQ, England

J. J. Brehm
Department of Physics and Astronomy, University of Massachusetts, Amherst, Massachusetts 01003
(Received 21 February 1978)

The isobar model for a production amplitude is developed in a construction which incorporates unitarity and analyticity in each of the two-body isobar subenergy channels. The process $KN \to K\pi N$ is considered in order to illustrate and deal with the complications due to spin and unequal masses. The basic aspects of the description are presented in a truncation of the problem to the production of s-wave isobars. The two-body discontinuities in each isobar channel have been derived previously, and are employed here in dispersion relations for the isobar factor amplitudes. A prominent complicating feature is that due to half-angle kinematics; this is investigated without approximation, and factors associated with kinematical singularities are identified and extracted. A coupled system of single-variable integral equations for the isobar factors is obtained by means of a procedure due to Pasquier and Pasquier. The kernels of the integral equations are evaluated explicitly. These contain the two-body elastic amplitudes in each isobar channel, the parametrization of which propagates into the solution for the isobar production amplitudes. The formal solution of the linear system of equations for the isobar factors is indicated. The final result is unitary and analytic in each subenergy and satisfies two-body unitarity in the total energy as well.

I. INTRODUCTION

A problem of early concern in high-energy physics has been that of constructing the amplitude for the two-body-to-three-body production process. In the past the methods of S-matrix theory have been applied to some extent by several authors.[1] Another early approach employed the isobar decomposition of the final state.[2] The latter scheme with its subsequent refinements[3] has been used extensively in phenomenology.[4] Recent progress in the development of this subject has stemmed from a marriage of these approaches, that is of unitary methods with isobar methods. Figure 1 illustrates the line of reasoning: In Fig. 1(a) the production amplitude in its isobar expansion is shown. Each isobar amplitude may then be expressed in product form as in Fig. 1(b), in which the elastic two-body amplitude occurs multiplied by an isobar factor. In simple isobar models, this isobar factor is taken to be independent of the subenergy variable. However, Fig. 1(c) illustrates the result of imposing unitarity on the full amplitude; the isobar factor has a nonzero discontinuity in the subenergy variable, and models in which this factor is subenergy-independent therefore violate unitarity. The importance of examining the results of subenergy unitarity in this way has been especially emphasized by Aaron and Amado.[5] The subenergy discontinuity of an isobar factor in a given channel is determined by the isobar factors in the other two channels, and a coupled system of constraints results. To implement these constraints properly, the discontinuities must be inserted into dispersion relations for the isobar factors; otherwise, spurious singularities in the isobar amplitudes may appear.[6] The combination of unitarity and analyticity then results in a "minimal" dynamical formalism for the three-hadron system.[7,8]

This approach has been fully implemented relativistically in a recent investigation of the 3π

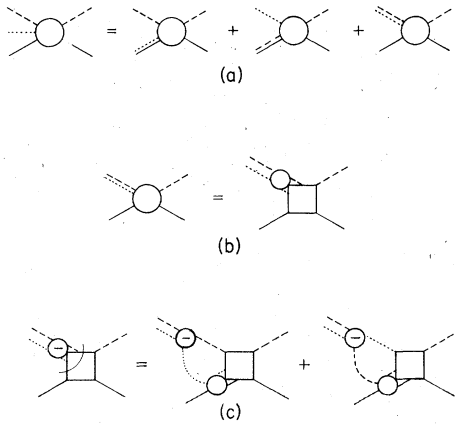

FIG. 1. (a) Expansion of the production amplitude into isobar amplitudes. (b) Isobar amplitude in product form; the amplitude for elastic scattering in the isobar channel is multiplied by an isobar factor amplitude. (c) Subenergy discontinuity of an isobar factor, expressed in terms of the isobar factors in the other two isobar channels.

problem.[9,10] The formalism appropriate when a particle has spin has also been developed[11,12] and the subenergy discontinuities for such processes have been derived. It is the purpose of the present work to undertake the next formal step for the latter problem, specifically, to show how the results of Ref. 11 are to be employed in order to express the constraints which follow from unitarity and analyticity in the form of integral equations in a *single* variable. To explain the emphasis here it should be recalled (see, e.g., Ref. 11) that the discontinuities themselves are integrals in a single variable ranging across the Dalitz plot and adjacent kinematic regions. Therefore, when these discontinuities are inserted into dispersion relations, integral equations in two variables are obtained directly. The passage to single-variable integral equations (which are, of course, more tractable for solution) is effected by first inverting the order of double integration. This step is carried out by means of a very clever procedure due to Pasquier and Pasquier.[13] The inversion produces explicit kinematic integrals which can be evaluated to form part of the kernel of the resulting single-variable integral equations. While the procedure is relatively straightforward for equal-mass spinless particles, both spin and unequal-mass kinematics lead to nontrivial complications.

In Sec. II the problem is laid out, preparatory to performing the inversion of the orders of integrations. The kinematical details are developed here for handling the combinations of half-angle functions which arise for spin-$\frac{1}{2}$ particles. In Sec. III the Pasquier inversion[13] is described, for the unequal mass case. In Sec. IV the kernels of the single-variable integral equations are identified explicitly, and the method of solution is indicated.

The treatment given in Ref. 11, which this work follows, contains an error which should be noted. The necessary corrections associated with this error, an overlooked phase factor, are given in an Appendix. In particular, the corrected version for Eqs. (B5)–(B7) of Ref. 11 is to be found there.

II. THE DISCONTINUITIES

The process $KN \to K\pi N$ was selected for illustration in Ref. 11; the notation of that paper is adopted here with little exception. As summarized in Fig. 2, the invariant mass variables are $s = W^2$, $s_1 = w_1^2$, $s_2 = w_2^2$, and $s_3 = w_3^2$, corresponding to total energy W, and isobar subenergies w_1, w_2, and w_3 for the final state πN, KN, and $K\pi$ isobars, respectively. (s_3 was called x in Ref. 11.) These invariants satisfy

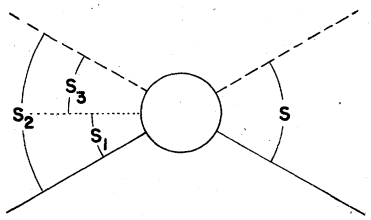

FIG. 2. Invariants for the process $KN \to K\pi N$.

$$s_1 + s_2 + s_3 = s + M^2 + m^2 + \mu^2 , \tag{1}$$

where M, m, and μ are the N, K, and π masses. Each isobar amplitude having definite angular momentum and parity J^P, and definite isobar spin and parity is expressed as in Fig. 1(b): For isobar channels 1 and 2

$$M^{J^P j^{\mathfrak{p}} \kappa}(W,w) = M^{j^{\mathfrak{p}}}(w)\mathfrak{M}^{J^P j^{\mathfrak{p}} \kappa}(W,w) ,$$

and (2)

$$M^{J^P l\,\xi}(W,w_3) = M^{l}(w_3)\mathfrak{M}^{J^P l\,\xi}(W,w_3)$$

for isobar channel 3. The extra index in each case, κ and ξ, refers to the $j + \frac{1}{2}$ and $2l+1$ independent amplitudes of definite J^P. The amplitudes also have definite total isospin and isobar isospin; the corresponding indices have been suppressed. When these expressions are inserted in Eqs. (A1)–(A3), the subenergy discontinuities of the $\mathfrak{M}$'s, the isobar factors, are obtained in the form suggested by Fig. 1(c). The coupled system of amplitudes is obviously quite complex when many isobar contributions are taken into account.

In order to focus upon the procedure for obtaining single-variable integral equations, it is sufficient to assume circumstances in which only s-wave systems need to be considered. If each isobar is in an s state with the third particle, and if there occur only the $j^{\mathfrak{p}} = \frac{1}{2}^-$ πN and KN isobars, and the $l = 0$ $K\pi$ isobar, then only $J^P = \frac{1}{2}^+$ is needed. There are then only three coupled isobar factors (apart from the multiplicity due to isospin), one for each isobar channel. The subenergy discontinuities are

$$\mathrm{disc}_1\mathfrak{M}_1 = 2\pi i \rho_1 \int d\cos\vartheta_1 \tfrac{1}{2}\left(\cos\frac{\epsilon_1+\epsilon_2}{2}(M_2\mathfrak{M}_2)_C + \cos\frac{\epsilon_1}{2}(M_3\mathfrak{M}_3)_C\right), \tag{3}$$

$$\mathrm{disc}_2\mathfrak{M}_2 = 2\pi i \rho_2 \int d\cos\vartheta_2 \tfrac{1}{2}\left(\cos\frac{\epsilon_1+\epsilon_2}{2}(M_1\mathfrak{M}_1)_C + \cos\frac{\epsilon_2}{2}(M_3\mathfrak{M}_3)_C\right), \tag{4}$$

$$\mathrm{disc}_3\mathfrak{M}_3 = 2\pi i\,\rho_3 \int d\cos\vartheta_3 \tfrac{1}{2}\left(\cos\frac{\epsilon_1}{2}\,(M_1\mathfrak{M}_1)_C + \cos\frac{\epsilon_2}{2}\,(M_2\mathfrak{M}_2)_C\right) \tag{5}$$

in which the angles ϵ_1 and ϵ_2 are given by

$$\epsilon_1 = \vartheta_1 - \omega_1 - \chi_a \quad \text{and} \quad \epsilon_2 = \vartheta_2 - \omega_2 - \chi_b\,, \tag{6}$$

in terms of angles described in Ref. 11 and below. The quantities $\mathfrak{M}_i$ and M_i denote the $\mathfrak{M}(W, w_i)$ and $M(w_i)$ of Eqs. (2) with all superscripts suppressed. The notation disc_i means discontinuity in the sub-energy s_i. These results are essentially the same as Eqs. (85)–(87) of Ref. 11. The main difference (apart from the corrections noted in Appendix A) is that the spin rotation angles ω_1 and ω_2 have not been ignored here; it will become evident that there is good reason to retain them. The subscript C on the right-hand side of Eqs. (3)–(5) refers to the suppressed isospin dependence and serves as a reminder of the presence of an isospin crossing matrix (see Ref. 11). The phase-space factors are

$$\rho_1 = MQ_1/16\pi^3 w_1\,, \tag{7}$$

$$\rho_2 = MQ_2/16\pi^3 w_2 \tag{8}$$

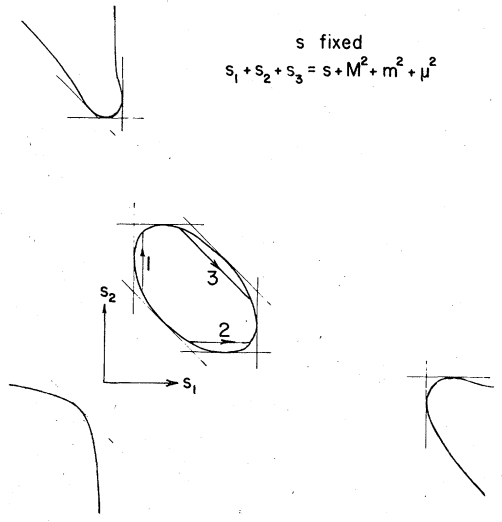

FIG. 3. Kinematic regions in the variables s_1, s_2, and s_3 with s fixed. The vertical lines from left to right denote the s_1 values: $(M-\mu)^2$, $(M+\mu)^2$, $(W-m)^2$, and $(W+m)^2$. The horizontal lines from bottom to top denote the s_2 values: $(M-m)^2$, $(M+m)^2$, $(W-\mu)^2$, and $(W+\mu)^2$. The diagonal lines from upper right to lower left denote the s_3 values: $(m-\mu)^2$, $(m+\mu)^2$, $(W-M)^2$, and $(W+M)^2$. The traversals of the Dalitz plot in the center refer to the integrations in Eqs. (3)–(5). The ith one indicates $\cos\vartheta_i$ ranging from -1 to 1 with s_i fixed.

$$\rho_3 = k_3/32\pi^3 w_3\,. \tag{9}$$

The momenta and angles are as in Ref. 11. Briefly, Q_1 (Q_2) is the N momentum in the πN (KN) isobar rest frame and k_3 is the K momentum in the $K\pi$ isobar rest frame; ϑ_1, ϑ_2, and ϑ_3 are the polar angles of the momenta Q_1, Q_2, and k_3. In the overall center-of-mass frame the momenta of the N, the πN isobar, and the KN isobar are, respectively, Q, Q_a, and Q_b. The angle χ_a (χ_b) is the one between Q and Q_a (Q_b).

The kinematic regions[14] associated with Fig. 2 are shown in Fig. 3. The Dalitz plot, or decay region, occupies the central portion, and the integrations in Eqs. (3)–(5) are indicated as traversals of this region. Some familiarity with Fig. 3 will prove to be invaluable for the procedures to follow. The procedures are to eliminate the angles in terms of the invariants and, once dispersion relations have been written, to invert the integration over the invariants.

Compared with the case of spinless particles, a problem with half-integral spin is evidently more complicated. One can see from Eqs. (3)–(5) that to confront even the simplest example is to encounter half-angle trigonometric functions of combinations of the angles $(\vartheta_1, \omega_1, \chi_a)$ and $(\vartheta_2, \omega_2, \chi_b)$. Because of this it would appear that grotesque square-root factors might afflict the equations. Fortunately this is not the case, and it is rather instructive to observe why these features are not so complicated as that.

It suffices to consider a term such as, say, $\sin\frac{1}{2}\vartheta_1 \sin\frac{1}{2}\omega_1 \cos\frac{1}{2}\chi_a$, and to show that it is expected, *a priori*, to be the square root of a perfect square. Of course this term is one of the four ingredients of the quantity $\cos\frac{1}{2}\epsilon_1$, which appears with others like it in Eqs. (3)–(5). For the momentum and energy variables Q and Q_0, Q_a and Q_{a0}, and Q_1 and Q_{10} the following dimensionless variables are notationally convenient:

$$P = Q/M\,, \quad P_0 = Q_0/M\,, \tag{10}$$

$$P_a = Q_a/w_1\,, \quad P_{a0} = Q_{a0}/w_1\,, \tag{11}$$

$$P_1 = Q_1/M\,, \quad P_{10} = Q_{10}/M\,; \tag{12}$$

these satisfy

$$P_0^2 - P^2 = P_{10}^2 - P_1^2 = P_{a0}^2 - P_a^2 = 1\,.$$

Expressions for the cosines of ϑ_1, ω_1, and χ_a can be written in terms of these[11]

$$\cos\vartheta_1 = (P_0 - P_{a0}P_{10})/P_aP_1\,, \tag{13}$$

$$\cos\omega_1 = (P_0P_{10} - P_{a0})/PP_1\,, \tag{14}$$

$$\cos\chi_a = (P_0P_{a0} - P_{10})/P_aP. \tag{15}$$

Figure 4(a) shows the Dalitz plot and the lines

touching it along which P, P_a, and P_1 vanish. It is apparent that $\cos\vartheta_1 = 1$ along the upper arc from A to C, that $\cos\omega_1 = 1$ along the longer arc from A to B, and that $\cos\chi_a = -1$ along the shorter arc from B to C. Therefore the factors $\sin\frac{1}{2}\vartheta_1$, $\sin\frac{1}{2}\omega_1$, and $\cos\frac{1}{2}\chi_a$ vanish with square-root behavior along these respective arcs. However, as shown in Fig. 4(b), these arcs overlap in such a way as to indicate that the product of the three factors vanishes like $(1-\cos\omega_1)$ over the longer arc from A to B. The desired result can in fact be obtained in two steps by showing first that

$$8\left(\sin\frac{\vartheta_1}{2}\sin\frac{\omega_1}{2}\cos\frac{\chi_a}{2}\right)^2 = \left(\frac{1-\cos\omega_1}{P_a}\right)^2 (PP_1P_{a0}+PP_aP_{10}+P_aP_1P_0+P_0P_{a0}P_{10}-1),$$

and then that

$$(PP_1P_{a0}+PP_aP_{10}+P_aP_1P_0+P_0P_{a0}P_{10}-1) = [(P_0+P)(P_{10}+P_1)(P_{a0}+P_a)-1]^2/2(P_0+P)(P_{10}+P_1)(P_{a0}+P_a).$$

The final result contains only simple kinematic root factors:

$$\sin\frac{\vartheta_1}{2}\sin\frac{\omega_1}{2}\cos\frac{\chi_a}{2} = \frac{1}{4}\frac{(PP_1-P_0P_{10}+P_{a0})}{PP_1P_a}\frac{[(P_0+P)(P_{10}+P_1)(P_{a0}+P_a)-1]}{(P_0+P)^{1/2}(P_{10}+P_1)^{1/2}(P_{a0}+P_a)^{1/2}}.$$

All the required triple products of half-angle functions behave in this way; as in Fig. 4(b), a complete overlap of three arcs occurs in each case corresponding to a coalescence of all offending square roots. At this point it is clear why the ω dependence should not be ignored (as one might be tempted to do in a low energy approximation): without the ω-dependent factor in the triple product the remaining two arcs, as in Fig. 4(b), fail to have a complete overlap so that the square roots do not completely coalesce.

The problem of dealing with the half-angle functions is entirely resolved by the foregoing discussion. It is then a matter of further algebra to obtain expressions for all the angle-dependent coefficients in Eqs. (3)–(5). In terms of the factor

$$U_1 = \frac{(P_0+P-1)(P_{10}+P_1-1)(P_{a0}+P_a-1)}{4PP_1P_a(P_0+P)^{1/2}(P_{10}+P_1)^{1/2}(P_{a0}+P_a)^{1/2}}$$

it can be shown that

$$\cos\frac{\epsilon_1}{2} = U_1(P_0+P_{10}+P_{a0}+1) \tag{16}$$

and

$$\sin\frac{\epsilon_1}{2} = U_1\phi^{1/2}/2Ww_1M. \tag{17}$$

To obtain the corresponding functions of ϵ_2, the replacements $1\to 2$ and $a\to b$ are made. The factor ϕ in Eq. (17) is

$$\begin{aligned}\phi &= 4ss_1M^2(2P_0P_{10}P_{a0}-P_0^2-P_{10}^2-P_{a0}^2+1)\\ &= 4ss_2M^2(2P_0P_{20}P_{b0}-P_0^2-P_{20}^2-P_{b0}^2+1).\end{aligned} \tag{18}$$

It then follows immediately that

$$\cos\frac{\epsilon_1+\epsilon_2}{2} = U_1U_2[(P_0+P_{10}+P_{a0}+1)(P_0+P_{20}+P_{b0}+1) - \phi/4sw_1w_2M^2]. \tag{19}$$

Note that P_2, P_{20}, P_b, and P_{b0} are defined in analogy with (11) and (12). The quantity ϕ is recognized as the Kibble cubic boundary function[14]; the boundary of the kinematic regions in Fig. 3 is given by the equation $\phi = 0$. In terms of the invariants it is written as

$$\begin{aligned}\phi &= s_1s_2s_3 - s_1(M^2\mu^2+sm^2) - s_2(M^2m^2+s\mu^2)\\ &\quad - s_3(m^2\mu^2+sM^2)\\ &\quad + 2(M^2m^2\mu^2+sM^2m^2+sM^2\mu^2+sm^2\mu^2).\end{aligned} \tag{20}$$

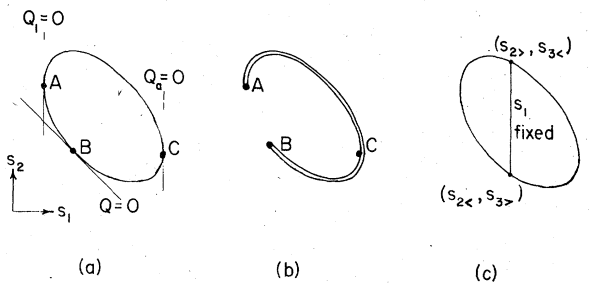

FIG. 4. (a) Dalitz plot and the lines along which the momenta Q, Q_a, and Q_1 vanish. (b) Arcs along which $\sin\frac{1}{2}\vartheta_1$, $\sin\frac{1}{2}\omega_1$, and $\cos\frac{1}{2}\chi_a$ vanish with square root behavior, respectively: arc AC, arc AB, and arc BC. Complete overlap of the arcs implies coalescence of the square roots in the triple product $\sin\frac{1}{2}\vartheta_1\sin\frac{1}{2}\omega_1\cos\frac{1}{2}\chi_a$. (c) Integration in $\cos\vartheta_1$ with s_1 fixed. The end points lie on the boundary curve where the function ϕ of Eq. (20) vanishes. Shown in the figure are the limits of integration appearing in Eq. (27).

The angles in Eqs. (3)–(5) are eliminated altogether by recalling[11] finally that

$$\frac{d\cos\vartheta_1}{ds_2} = -\frac{d\cos\vartheta_1}{ds_3} = \frac{w_1}{2WQ_aQ_1} \quad (s_1 \text{ fixed}), \tag{21}$$

$$\frac{d\cos\vartheta_2}{ds_1} = -\frac{d\cos\vartheta_2}{ds_3} = \frac{w_2}{2WQ_bQ_2} \quad (s_2 \text{ fixed}), \tag{22}$$

$$\frac{d\cos\vartheta_3}{ds_1} = -\frac{d\cos\vartheta_3}{ds_2} = \frac{w_3}{2WQk_3} \quad (s_3 \text{ fixed}). \tag{23}$$

The kinematic square roots in U_1 and U_2 which show up in Eqs. (16) and (19) may be systematically absorbed in the definition of new amplitudes. The isobar factors $\mathfrak{M}_i$ and the new amplitudes G_i may be related as follows:

$$G_1 = \frac{P_{10}+P_1+1}{(P_{10}+P_1)^{1/2}} \frac{P_{a0}+P_a+1}{(P_{a0}+P_a)^{1/2}} \mathfrak{M}_1, \tag{24}$$

$$G_2 = \frac{P_{20}+P_2+1}{(P_{20}+P_2)^{1/2}} \frac{P_{b0}+P_b+1}{(P_{b0}+P_b)^{1/2}} \mathfrak{M}_2, \tag{25}$$

$$G_3 = \frac{P_0+P+1}{(P_0+P)^{1/2}} \mathfrak{M}_3. \tag{26}$$

The kinematic factors above have the property that they have no discontinuities on the two-body cuts; for example,

$$\operatorname{disc}_1 \frac{P_{10}+P_1+1}{(P_{10}+P_1)^{1/2}} = \operatorname{disc}_1[(P_{10}+P_1)^{1/2} + (P_{10}-P_1)^{1/2}] = 0.$$

When Eqs. (7)–(9), (16), (19), (21)–(23), and (24)–(26) are incorporated into Eqs. (3)–(5), the discontinuity relations take the form

$$\frac{1}{2i}\operatorname{disc}_1 G_1 = \int_{s_{2<}(s_1)}^{s_{2>}(s_1)} ds_2 \Phi_{12}(M_2 G_2)_C + \int_{s_{3<}(s_1)}^{s_{3>}(s_1)} ds_3 \Phi_{13}(M_3 G_3)_C, \tag{27}$$

$$\frac{1}{2i}\operatorname{disc}_2 G_2 = \int_{s_{1<}(s_2)}^{s_{1>}(s_2)} ds_1 \Phi_{21}(M_1 G_1)_C + \int_{s_{3<}(s_2)}^{s_{3>}(s_2)} ds_3 \Phi_{23}(M_3 G_3)_C, \tag{28}$$

$$\frac{1}{2i}\operatorname{disc}_3 G_3 = \int_{s_{1<}(s_3)}^{s_{1>}(s_3)} ds_1 \Phi_{31}(M_1 G_1)_C + \int_{s_{2<}(s_3)}^{s_{2>}(s_3)} ds_2 \Phi_{32}(M_2 G_2)_C. \tag{29}$$

The end points of the traversals of the Dalitz plot shown in Fig. 3 correspond to the limits of integration above. For example the points $s_{2\gtrless}(s_1)$ and $s_{3\gtrless}(s_1)$ are as indicated in Fig. 4(c). The Φ's in Eqs. (27)–(29) contain all the accumulated kinematic factors

$$\Phi_{12} = \frac{M}{128\pi^2 WQ_a} \frac{(P_0+P_{10}+P_{a0}+1)(P_0+P_{20}+P_{b0}+1) - \phi/4sw_1w_2M^2}{(P_0+1)(P_{20}+1)(P_{b0}+1)}, \tag{30}$$

$$\Phi_{13} = \frac{M}{64\pi^2 WQ_a} \frac{P_0+P_{10}+P_{a0}+1}{P_0+1}, \tag{31}$$

$$\Phi_{21} = \frac{M}{128\pi^2 WQ_b} \frac{(P_0+P_{10}+P_{a0}+1)(P_0+P_{20}+P_{b0}+1) - \phi/4sw_1w_2M^2}{(P_0+1)(P_{10}+1)(P_{a0}+1)}, \tag{32}$$

$$\Phi_{23} = \frac{M}{64\pi^2 WQ_b} \frac{P_0+P_{20}+P_{b0}+1}{P_0+1}, \tag{33}$$

$$\Phi_{31} = \frac{1}{256\pi^2 WQ} \frac{P_0+P_{10}+P_{a0}+1}{(P_{10}+1)(P_{a0}+1)}, \tag{34}$$

$$\Phi_{32} = \frac{1}{256\pi^2 WQ} \frac{P_0+P_{20}+P_{b0}+1}{(P_{20}+1)(P_{b0}+1)}. \tag{35}$$

These quantities may be expressed in terms of the invariants by means of Eqs. (65)–(72) of Ref. 11; the function Φ_{ij} depends on the invariants s_i, s_j, and s.

Dispersion relations may now be written in the isobar subenergy variable for each of the amplitudes:

$$G_i - \bar{G}_i = \frac{1}{\pi} \int_{\text{thres}\,i}^{\infty} \frac{dz_i}{z_i - s_i} \frac{1}{2i} \operatorname{disc}_i G_i \tag{36}$$

in which the $\bar{G}_i$'s are functions of s, independent of s_i.

The construction of the G amplitudes at this

point follows from the solution of coupled integral equations in two variables. The crucial inversion[13] of the orders of double integration is the next step.

III. THE PASQUIER INVERSION

It suffices to show how the method of Ref. 13 is used to invert one of the double integrals arising from Eq. (36). The one selected is

$$G_1-\bar{G}_1=\frac{1}{\pi}\int_{(M+\mu)^2}^{\infty}\frac{dz_1}{z_1-s_1}\times\left(\int_{s_{2<}(z_1)}^{s_{2>}(z_1)}dz_2\Phi_{12}(M_2G_2)_C+\int_{s_{3<}(z_1)}^{s_{3>}(z_1)}dz_3\Phi_{13}(M_3G_3)_C\right),\tag{37}$$

in which the variables in the integrands are z_1, z_2, and z_3; s_1 is assigned a value below threshold. The limits of integration, as in Fig. 4(c), must be continued analytically as z_1 increases to values outside the Dalitz plot. For z_1 in the range $(W-m)^2$ to $(W+m)^2$, these limits are complex conjugate points in the z_2 and z_3 planes; for $z_1 \geq (W+m)^2$ the limits return to the real axis. The paths followed by $s_{2<}$ and $s_{2>}$ as z_1 increases from $(M+\mu)^2$ to ∞ are shown in Fig. 5; the motion of these 2 points is readily obtained by examining the boundary curve in Fig. 3.

The procedure begins by recognizing, with Pasquier and Pasquier,[13] that (37) can be re-expressed in terms of contour integrals in two complex planes:

$$G_1-\bar{G}_1=\frac{1}{\pi}\int_{C_1}\frac{dz_1}{z_1-s_1}\left(\int_{\Gamma_2(\tilde{s}_2)}dz_2\Phi_{12}(M_2G_2)_C+\int_{\Gamma_3(\tilde{s}_3)}dz_3\Phi_{13}(M_3G_3)_C\right).\tag{38}$$

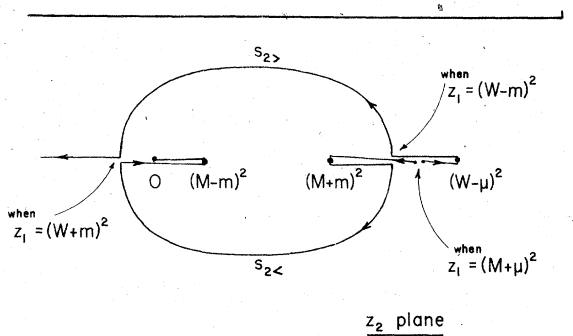

FIG. 5. Paths followed by the limits of integration $s_{2<}(z_1)$ and $s_{2>}(z_1)$ in Eq.(37), as z_1 increases from $(M+\mu)^2$ to ∞. For z_1 between $(W-m)^2$ and $(W+m)^2$, $s_{2<}$ and $s_{2>}$ are complex.

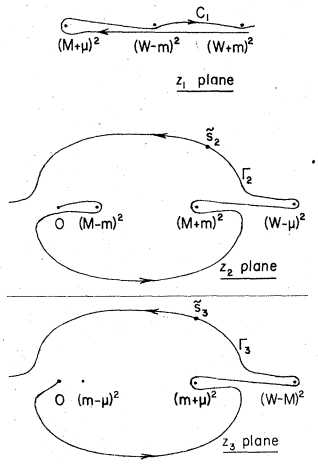

FIG. 6. Integration paths for Eq. (38). For each z_1 in the integration over C_1, the z_2 and z_3 integrations run over contours from 0 to the point $\tilde{s}_2$ on Γ_2 and $\tilde{s}_3$ on Γ_3, respectively. In the text these contours are denoted as $\Gamma_2(\tilde{s}_2)$ and $\Gamma_3(\tilde{s}_3)$. The locations of $\tilde{s}_2$ and $\tilde{s}_3$ are shown for a value of z_1 on C_1 above the real axis between $(W-m)^2$ and $(W+m)^2$. As z_1 runs the length of C_1, $\tilde{s}_2$ and $\tilde{s}_3$ sweep out all of Γ_2 and Γ_3. Note how the right-most point in the z_2 and the z_3 plane is encircled, due to the fixed $s+i0$ stipulation.

To see this, consider the double integral over z_1 and z_2 in (37) and start with the simple observation that (suppressing the integrands)

$$\int_{s_{2<}(z_1)}^{s_{2>}(z_1)}dz_2=\int_0^{s_{2>}(z_1)}dz_2-\int_0^{s_{2<}(z_1)}dz_2.$$

Then, given $s+i0$, introduce the contour C_1 in the z_1 plane as shown in Fig. 6 and make the following correspondence. For each real z_1 in (37) assign the limit $s_{2>}(z_1)$ $[s_{2<}(z_1)]$ to z_1+i0 (z_1-i0) on the portion of C_1 above (below) the real z_1 axis. The point in the z_2 plane, call it $\tilde{s}_2(z_1)$, assigned in this way, follows the path Γ_2 in Fig. 6; for each z_1 on C_1 the z_2 integration runs along Γ_2 from 0 to $\tilde{s}_2$. The notation $\Gamma_2(\tilde{s}_2)$ in (38) refers to this contour of integration. The end point $\tilde{s}_2$ sweeps out all of Γ_2 as z_1 runs over the length of C_1. The double integral over z_1 and z_3 is treated in similar fashion; $\Gamma_3(\tilde{s}_3)$ in the z_3 plane is analogous to $\Gamma_2(\tilde{s}_2)$ in the z_2 plane.

The procedure continues by reversing the order of integration while observing the correspondence that has been set up between the variables:

$$\frac{1}{\pi}\int_{C_1}\frac{dz_1}{z_1-s_1}\int_{\Gamma_2(\tilde{s}_2)}dz_2=\int_{\Gamma_2}dz_2\frac{1}{\pi}\int_{C_1(\tilde{s}_1)}\frac{dz_1}{z_1-s_1}.$$

For each z_2 on Γ_2, the z_1 integration follows the portion of C_1 which begins at the corresponding

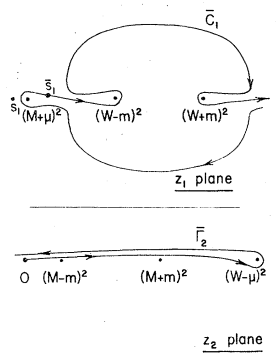

FIG. 7. Deformation of contours after reversing the order of integration. The point $\bar{s}_1$ shown on $\bar{C}_1$ corresponds to a value of z_2 on $\bar{\Gamma}_2$ near $(W-\mu)^2$. For this value of z_2 the z_1 integration runs along $\bar{C}_1$ from $\bar{s}_1$ to $+\infty$ above the real axis. In the text this contour of integration is denoted as $\bar{C}_1(\bar{s}_1)$.

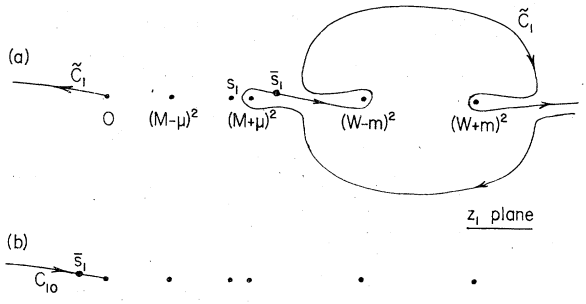

FIG. 9. (a) Path $\tilde{C}_1$, followed by $\bar{s}_1$ as z_2 runs along $\tilde{\Gamma}_2$. $\tilde{C}_1$ differs from $\bar{C}_1$ by the addition of the piece from 0 to $-\infty$. The contour $\tilde{C}_1(\bar{s}_1)$ in the text runs from $\bar{s}_1$ to $+\infty$. (b) Path C_{10} followed by $\bar{s}_1$ as z_2 runs along Γ_{20}. The contour $C_{10}(\bar{s}_1)$ in the text runs from $\bar{s}_1$ to $-\infty$. Note that the direction of the contour $C_{10}(\bar{s}_1)$ is opposite to the direction of the path of motion of $\bar{s}_1$, C_{10}, show in the figure.

value of z_1, called $\bar{s}_1$ in the equation above, and runs to $+\infty$ on top of the real axis. The double integral in this form may now be subjected to contour deformation. Γ_2 is collapsed to the real z_2 axis; because of the correspondence C_1 must be opened up compatibly. Then one obtains

$$\int_{\Gamma_2} dz_2 \frac{1}{\pi} \int_{C_1(\bar{s}_1)} \frac{dz_1}{z_1 - s_1} = \int_{\bar{\Gamma}_2} dz_2 \frac{1}{\pi} \int_{\bar{C}_1(\bar{s}_1)} \frac{dz_1}{z_1 - s_1} .$$

The resulting contours are indicated in Fig. 7. For each z_2 on $\bar{\Gamma}_2$, the z_1 integration runs from the corresponding point $\bar{s}_1$ on $\bar{C}_1$ to $+\infty$ above the real axis; this contour is denoted as $\bar{C}_1(\bar{s}_1)$ above. $\bar{\Gamma}_2$ can itself be deformed toward $-\infty$ in the z_2 plane, as shown in Fig. 8, to obtain the configuration consisting of the two pieces $\tilde{\Gamma}_2$ and Γ_{20}. This step is expressed as

$$\int_{\bar{\Gamma}_2} dz_2 \frac{1}{\pi} \int_{\bar{C}_1(\bar{s}_1)} \frac{dz_1}{z_1 - s_1} = \int_{\tilde{\Gamma}_2} dz_2 \frac{1}{\pi} \int_{\tilde{C}_1(\bar{s}_1)} \frac{dz_1}{z_1 - s_1} + \int_{\Gamma_{20}} dz_2 \frac{1}{\pi} \int_{C_{10}(\bar{s}_1)} \frac{dz_1}{z_1 - s_1} ,$$

the explanation of which follows, with the aid of Figs. 8 and 9. For each z_2 on the contour $\tilde{\Gamma}_2$, the z_1 integration again runs from the corresponding

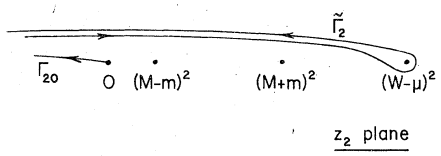

FIG. 8. Deformation of the contour $\bar{\Gamma}_2$ into the two pieces $\tilde{\Gamma}_2$ and Γ_{20}.

$\bar{s}_1$ to $+\infty$; here, however, the path $\tilde{C}_1$ over which $\bar{s}_1$ ranges includes $\bar{C}_1$ and also a new piece from 0 to $-\infty$, arising from the deformation of $\bar{\Gamma}_2$. This new piece is countered in the second term above; for each z_2 on Γ_{20}, the z_1 contour runs from the corresponding $\bar{s}_1$ to $-\infty$ along C_{10}. Thus the contours $\tilde{C}_1(\bar{s}_1)$ and $C_{10}(\bar{s}_1)$ in the expression above follow the paths in Fig. 9, denoted as $\tilde{C}_1$ and C_{10}, from $\bar{s}_1$ to $+\infty$ and from $\bar{s}_1$ to $-\infty$, respectively.

The procedure concludes by expressing the contour integrations of Fig. 8 in terms of the contributions of the two contours α_2 and γ_2 in the z_2 plane which run from $-\infty$ to the points $(W-\mu)^2$ and 0, respectively, as shown in Fig 10(a). Clearly γ_2 is just Γ_{20} in reverse so the z_1 integration is over $C_{10}(\bar{s}_1)$ in reverse, a contour indicated as L_{12} in Fig. 10(b). At each z_2 on α_2, the difference

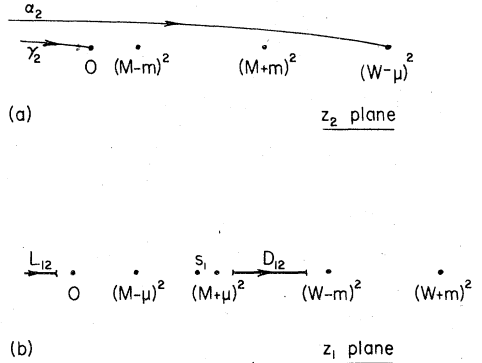

FIG. 10. (a) Contours α_2 and γ_2 obtained from $\tilde{\Gamma}_2$ and Γ_{20}. (b) Contours in the z_1 plane which appear in result (39). D_{12} is shown for a choice of z_2 on α_2 near $(W-\mu)^2$; L_{12} is shown for a choice of z_2 on γ_2 near 0.

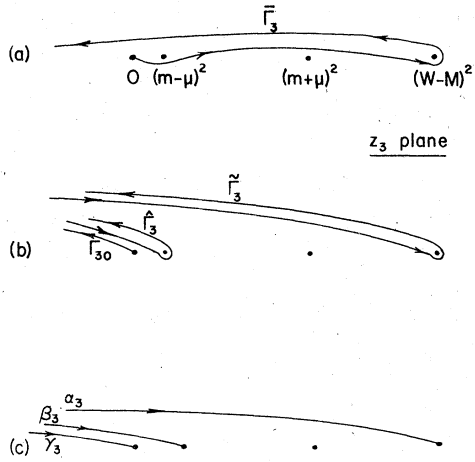

FIG. 11. (a) Γ_3 of Fig. 6 is flattened to become $\bar{\Gamma}_3$. (b) $\bar{\Gamma}_3$ is deformed toward $-\infty$ to obtain three contours $\tilde{\Gamma}_3$, $\hat{\Gamma}_3$, and Γ_{30}. (c) Final contours in the z_3 plane leading to result (40).

is taken between branches of $\tilde{\Gamma}_2$. That is, for each z_2 on α_2, the z_1 integration starts from $\bar{s}_1(z_2 - i0)$ and ends at $\bar{s}_1(z_2 + i0)$ corresponding to the points $z_2 \pm i0$ on the two branches of $\bar{\Gamma}_2$. The resulting z_1 contour is indicated as D_{12} in Fig. 10(b). This final step is expressed as

$$\int_{\tilde{\Gamma}_2} dz_2 \frac{1}{\pi} \int_{\tilde{C}_1(\bar{s}_1)} \frac{dz_1}{z_1 - s_1} = \int_{\alpha_2} dz_2 \frac{1}{\pi} \int_{D_{12}} \frac{dz_1}{z_1 - s_1}$$

and

$$\int_{\Gamma_{20}} dz_2 \frac{1}{\pi} \int_{C_{10}(\bar{s}_1)} \frac{dz_1}{z_1 - s_1} = \int_{\gamma_2} dz_2 \frac{1}{\pi} \int_{L_{12}} \frac{dz_1}{z_1 - s_1} .$$

In Fig. 10(b), Γ_{12} and L_{12} have been indicated for values of z_2 near the right end points of α_2 and γ_2 [i.e., near $(W-\mu)^2$ and 0], respectively.

By this sequence of steps the first double integral in Eq. (37) is manipulated into the form

$$\int_{-\infty}^{(W-\mu)^2} dz_2 \left(\frac{1}{\pi} \int_{D_{12}} \frac{dz_1}{z_1 - s_1} \Phi_{12} \right) (M_2 G_2)_C + \int_{-\infty}^{0} dz_2 \left(\frac{1}{\pi} \int_{L_{12}} \frac{dz_1}{z_1 - s_1} \Phi_{12} \right) (M_2 G_2)_C . \quad (39)$$

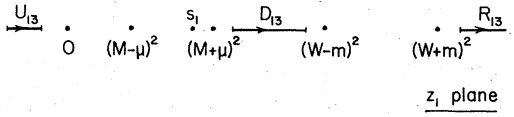

FIG. 12. Contours in the z_3 plane which appear in result (40). D_{13} is shown for a choice of z_3 on α_3 near $(W-M)^2$, U_{13} for a choice of z_3 on β_3 near $(m-\mu)^2$, and R_{13} for a choice of z_3 on γ_3 near 0.

The advantage of achieving this result is obvious. The factors in brackets in (39) are integrals over explicit kinematic functions. Once integrated these factors provide for the kernels of the resulting *single-variable* integral equations for the G amplitudes.

The double integral over z_1 and z_3 in (37) and (38) is manipulated according to the same procedure, but with an important extra feature. In Fig. 6, accompanying Eq. (38), the contour Γ_3 in the z_3 plane leaves the origin in a different fashion than Γ_2 does. When Γ_3 is deformed to obtain $\bar{\Gamma}_3$, the additional point $z_3 = (m-\mu)^2$ is picked up, as in Fig. 11(a). This gives rise to three contours in the deformation of $\bar{\Gamma}_3$ into $\tilde{\Gamma}_3$, $\hat{\Gamma}_3$, and Γ_{30}, shown in Fig. 11(b). Finally, three contours appear in the final form: α_3, β_3, and γ_3 as shown in Fig. 11(c). When the Pasquier procedure is implemented with these steps, it is straightforward to show that the second double integral in Eq. (37) is manipulated into the form

$$\int_{-\infty}^{(W-M)^2} dz_3 \left(\frac{1}{\pi} \int_{D_{13}} \frac{dz_1}{z_1 - s_1} \Phi_{13} \right) (M_3 G_3)_C + \int_{-\infty}^{(m-\mu)^2} dz_3 \left(\frac{1}{\pi} \int_{U_{13}} \frac{dz_1}{z_1 - s_1} \Phi_{13} \right) (M_3 G_3)_C - \int_{-\infty}^{0} dz_3 \left(\frac{1}{\pi} \int_{R_{13}} \frac{dz_1}{z_1 - s_1} \Phi_{13} \right) (M_3 G_3)_C . \quad (40)$$

The contours in the z_1 integrations are as shown in Fig. 12.

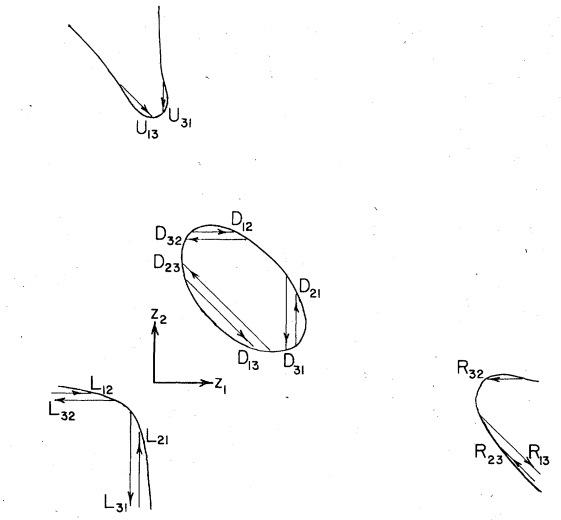

FIG. 13. Contours for the evaluation of the kernels $\mathfrak{D}_{ij}$, $\mathfrak{U}_{ij}$, $\mathfrak{L}_{ij}$, and $\mathfrak{R}_{ij}$. The contours D_{ij}, U_{ij}, L_{ij}, and R_{ij} are indicated by traversals of the kinematic regions in the variable z_i with z_j fixed.

The contours associated with the kernels in Eqs. (39) and (40) are more easily visualized in terms of the Dalitz plot and the adjacent kinematic regions. Figure 13 shows a map of all such contours for all the kernels in the problem, each one represented as a traversal of the relevant kinematic region. In each case the traversal is shown for a given value of the other fixed variable near its upper limit. As this fixed variable sweeps down its range, the evaluated kernels can then be obtained by analytic continuation. All roots occurring in the Φ functions are specified to have positive values when the variables lie inside the decay region; outside, the branches are determined by analytic continuation.

The Pasquier inversion applied to each double integral arising from Eq. (36) leads to the following results:

$$G_1 - \bar{G}_1 = \int_{-\infty}^{(W-\mu)^2} dz_2 \mathfrak{D}_{12}(M_2 G_2)_C + \int_{-\infty}^{0} dz_2 \mathfrak{L}_{12}(M_2 G_2)_C + \int_{-\infty}^{(W-M)^2} dz_3 \mathfrak{D}_{13}(M_3 G_3)_C + \int_{-\infty}^{(m-\mu)^2} dz_3 \mathfrak{U}_{13}(M_3 G_3)_C - \int_{-\infty}^{0} dz_3 \mathfrak{R}_{13}(M_3 G_3)_C , \tag{41}$$

$$G_2 - \bar{G}_2 = \int_{-\infty}^{(W-m)^2} dz_1 \mathfrak{D}_{21}(M_1 G_1)_C + \int_{-\infty}^{0} dz_1 \mathfrak{L}_{21}(M_1 G_1)_C + \int_{-\infty}^{(W-M)^2} dz_3 \mathfrak{D}_{23}(M_3 G_3)_C + \int_{-\infty}^{0} dz_3 \mathfrak{R}_{23}(M_3 G_3)_C , \tag{42}$$

$$G_3 - \bar{G}_3 = \int_{-\infty}^{(W-m)^2} dz_1 \mathfrak{D}_{31}(M_1 G_1)_C + \int_{-\infty}^{(M-\mu)^2} dz_1 \mathfrak{U}_{31}(M_1 G_1)_C - \int_{-\infty}^{0} dz_1 \mathfrak{L}_{31}(M_1 G_1)_C + \int_{-\infty}^{(W-\mu)^2} dz_2 \mathfrak{D}_{32}(M_2 G_2)_C + \int_{-\infty}^{(M-m)^2} dz_2 \mathfrak{R}_{32}(M_2 G_2)_C - \int_{-\infty}^{0} dz_2 \mathfrak{L}_{32}(M_2 G_2)_C . \tag{43}$$

In Eqs. (41)–(43) the kernel $\mathfrak{D}_{ij}(s_i z_j)$ corresponds to the contour D_{ij}; it is

$$\mathfrak{D}_{ij} = \frac{1}{\pi} \int_{D_{ij}} \frac{dz_i}{z_i - s_i} \Phi_{ij} , \quad z_j \text{ fixed} ; \tag{44}$$

the other kernels correspond to the other contours: $\mathfrak{U}_{ij}$ to U_{ij}, $\mathfrak{L}_{ij}$ to L_{ij}, and $\mathfrak{R}_{ij}$ to R_{ij}. Figure 13 shows all of the necessary contours.

IV. THE INTEGRAL EQUATIONS AND THEIR SOLUTION

In order to examine the full structure of Eqs. (41)–(43), the isospin dependence should be recalled.[11] According to the notation T = total isospin, and t_i = isospin of isobar i, the integral equations in a single variable are

$$G_1^{Tt_1}(ss_1) = \bar{G}_1^{Tt_1}(s) + \sum_{t_2} \int_{-\infty}^{(W-\mu)^2} dz_2 K_{12}^{Tt_1 t_2}(ss_1 z_2) G_2^{Tt_2}(s z_2) + \sum_{t_3} \int_{-\infty}^{(W-M)^2} dz_3 K_{13}^{Tt_1 t_3}(ss_1 z_3) G_3^{Tt_3}(s z_3) , \tag{45}$$

$$G_2^{Tt_2}(ss_2) = \bar{G}_2^{Tt_2}(s) + \sum_{t_1} \int_{-\infty}^{(W-m)^2} dz_1 K_{21}^{Tt_2 t_1}(ss_2 z_1) G_1^{Tt_1}(s z_1) + \sum_{t_3} \int_{-\infty}^{(W-M)^2} dz_3 K_{23}^{Tt_2 t_3}(ss_2 z_3) G_3^{Tt_3}(s z_3) , \tag{46}$$

$$G_3^{Tt_3}(ss_3) = \bar{G}_3^{Tt_3}(s) + \sum_{t_1} \int_{-\infty}^{(W-m)^2} dz_1 K_{31}^{Tt_3 t_1}(ss_3 z_1) G_1^{Tt_1}(s z_1) + \sum_{t_2} \int_{-\infty}^{(W-\mu)^2} dz_2 K_{32}^{Tt_3 t_2}(ss_3 z_2) G_2^{Tt_2}(s z_2) . \tag{47}$$

The kernels are composed of three types of factors:

$$K_{ij}^{Tt_i t_j}(ss_i z_j) = H_{ij}(ss_i z_j) C_{t_i t_j}^{T} M_j^{t_j}(z_j) . \tag{48}$$

The H factors contain appropriately the terms $\mathfrak{D}$, $\mathfrak{U}$, $\mathfrak{L}$, and $\mathfrak{R}$ of Eqs. (41)–(43), as described below. The C's are the isospin crossing matrices of Ref. 11, Table I. The kernels also contain the two-body elastic amplitudes which satisfy the unitarity relations, Eqs. (45) and (56) of Ref. 11. For use in the isobar model the simplest form to adopt is the effective-range approximation:

$$M_j^{t_j} = (A_j^{t_j} - \zeta_j)^{-1} , \tag{49}$$

where $\zeta_j(z_j)$ is analytic, having only the right-hand cut in z_j on which $\mathrm{Im}\zeta_j = \pi\rho_j$. In (49), $A_j^{t_j}$ is a

polynomial in which there occur the constants which parametrize the two-body elastic scattering amplitudes.

It would appear, on inspection of Eqs. (41)–(43), that the H_{ij}'s are as follows:

$$H_{12} = \mathfrak{D}_{12} + \theta(-z_2)\mathfrak{L}_{12}\,,$$

$$H_{13} = \mathfrak{D}_{13} + \theta((m-\mu)^2 - z_3)\mathfrak{U}_{13} - \theta(-z_3)\mathfrak{R}_{13}\,,$$

etc.

A minor problem, which has not yet been made apparent, causes H_{ij} to be modified. The integrals $\mathfrak{L}_{ij}$ and $\mathfrak{R}_{ij}$ do not converge in their present form. The cure is readily found by reconsidering Eq. (36) and the role of $\bar{G}_i$, introduced there. It is clear that $\bar{G}_i$ serves as a subtraction constant insofar as the variable s_i is concerned, with subtraction point at $s_i = \infty$. This procedure fails if the integral over z_i is not convergent. The remedy then is to choose the subtraction point in the finite plane at $s_i = s_{i0}$, such that

$$\bar{G}_i = (G_i)_{s_i = s_{i0}}\,. \tag{50}$$

Then (36) is replaced by

$$G_i - \bar{G}_i = \frac{s_i - s_{i0}}{\pi}\int_{\text{threshold}_i}^{\infty} \frac{dz_i}{(z_i - s_i)(z_i - s_{i0})} \times \frac{1}{2i}\,\text{disc}_i G_i\,. \tag{51}$$

A convenient choice to make is in fact $s_{i0} = \text{threshold}_i$. All of Sec. III goes through, down to Eqs. (41)–(43), with the replacement

$$\int \frac{dz_i}{z_i - s_i}\Phi_{ij} \to (s_i - s_{i0})\int \frac{dz_i}{(z_i - s_i)(z_i - s_{i0})}\Phi_{ij}\,. \tag{52}$$

This amounts to the formal replacement

$$\mathfrak{D}_{ij}(s_i z_j) \to \mathfrak{D}_{ij}(s_i z_j) - \mathfrak{D}_{ij}(s_{i0} z_j)\,, \tag{53}$$

and similarly for $\mathfrak{U}_{ij}$, $\mathfrak{L}_{ij}$, and $\mathfrak{R}_{ij}$, wherever these functions occur in (41)–(43). The factor H_{ij} in (48) can now be identified, observing injunction (53). Because it is an integration in the variable z_i with z_j fixed, factors in it which depend only on s and z_j may be extracted. With the use of Eqs. (30)–(35), together with (52), H_{ij} takes the form

$$H_{ij}(s s_i z_j) = [I_{ij}(s s_i z_j) - I_{ij}(s s_{i0} z_j)]\, Z_j(s z_j) \tag{54}$$

in which

$$Z_1(s z_1) = M/[64\pi^3(P_{10}+1)(P_{a0}+1)]\,,$$

$$Z_2(s z_2) = M/[64\pi^3(P_{20}+1)(P_{b0}+1)]\,, \tag{55}$$

$$Z_3(s z_3) = M/[32\pi^3(P_0+1)]\,.$$

The remaining quantity I_{ij} contains the basic residual integrals, of two types, with certain rather lengthy kinematical factors:

$$I_{12} = \{1 + P_{20} + P_{b0} + [\sqrt{s_1}P_{10}(s_1) + \sqrt{z_2}P_{20} - M]/W\}\Delta_{12} + (\sqrt{s_1}[P_{10}(s_1) + P_{a0}(s_1)] + (W+M)(P_{20}+P_{b0}) + \sqrt{z_2}\{[\sqrt{s_1}P_{10}(s_1) + \sqrt{z_2}P_{20} - M]/W - 2P_{20}P_{b0} - 1\})\Gamma_{12}\,, \tag{56}$$

$$I_{13} = (1+P_0)\Delta_{13} + \sqrt{s_1}[P_{10}(s_1) + P_{a0}(s_1)]\Gamma_{13}\,, \tag{57}$$

$$I_{31} = (1/2M)[1 + P_0(s_3) + P_{10} + P_{a0}]\Delta_{31}\,; \tag{58}$$

I_{21}, I_{23}, and I_{32} are obtained from I_{12}, I_{13}, and I_{31}, respectively, with the substitution of subscripts $1 \leftrightarrow 2$ and $a \leftrightarrow b$. The basic integrals themselves are the factors Δ_{ij} and Γ_{ij} in (56)–(58). These are identified in Appendix B where the details of their explicit evaluation do not interfere with the flow of the text. A distressing feature of these results should be noted here, however. It turns out (see Appendix B) that Γ_{ij} is an elliptic integral of the third kind. Its appearance, which will considerably complicate the numerical treatment of the integral equations, may be traced directly to the $\sqrt{z_i}$ factors which occur inevitably due to the unequal-mass kinematics.

In the equal-mass case, it has been found[7,9] that the $\mathfrak{D}_{ij}$ parts of the kernels are equal to, or related to, partial wave projections (in the three-body system) of one-particle-exchange (OPE) graphs, in which the common particle is exchanged between the two isobar pairs having invariant masses $\sqrt{s_i}$ and $\sqrt{z_j}$. In the present case, it is clear that such projections will lead, as usual, to logarithmic functions and not to elliptic integrals. The reason for the discrepancy lies precisely in the factors $\sqrt{s_i}$ and $\sqrt{z_j}$. The OPE partial waves necessarily have singularities at $s_i = 0$ and $z_j = 0$ associated with these factors; however, the treatment which follows from (36) and (51) provides for isobar amplitudes having only the normal threshold branch points. It is shown in Appendix C that the physical region discontinuities of the $\mathfrak{D}_{ij}$ kernels are related to the corresponding discontinuities of the OPE partial waves. This correspondence suggests an approximation to the $\mathfrak{D}_{ij}$ part of the elliptic integral Γ_{ij} (denoted by $\Gamma_{D_{ij}}$ in Appendix B) which may be useful in practical applications: One simply replaces the factor $\sqrt{z_i}$ inside the integral by $\sqrt{s_i}$ outside. This maneuver preserves the physical region discontinuity but replaces $\sqrt{s_i}\Gamma_{D_{ij}}$ by the logarithmic function $\Delta^{(1)}_{ij}$ identified in Appendix B, the latter involving just the form of logarithm which arises in the corresponding OPE partial wave.

It has also been found,[7,9] in the equal-mass case, that the remaining parts of the kernels, analogous to the pieces identified here as $\mathfrak{U}_{ij}$, $\mathfrak{L}_{ij}$, and $\mathfrak{R}_{ij}$,

are related to certain internal mass discontinuities of the triangle graph in perturbation theory. In the present case, the substitution $\sqrt{z_i} \to \sqrt{s_i}$ throughout (i.e., $\Gamma_{ij} \to \Delta_{ij}/\sqrt{s_i}$) enables the integrals $\mathfrak{U}_{ij}$, $\mathfrak{L}_{ij}$, and $\mathfrak{R}_{ij}$ to be evaluated in terms of elementary functions which are just those occurring in the analysis[15] of the unequal-mass triangle graph. These integrals are also identified in Appendix B.

It is clear that the simplifying substitution, proposed above, will alter the analytic structure of the isobar amplitudes constructed according to (36) and (51); in particular, singularities at $s_i = 0$ will be introduced. It is unlikely that this will be a serious liability as far as results in the physical region are concerned. In any case, elimination of the elliptic integrals by some such simplifying step would seem to be necessary in any practical application of the formalism.

In Ref. 11 a further unitarity constraint was cited, namely, that associated with the two-body discontinuity in the total energy variable s. This takes the following form when applied to the G_i amplitudes (isospin suppressed):

$$\mathrm{disc}_s G_i = 2\pi i \rho G_i \hat{M}_- , \tag{59}$$

a result which follows directly from Eqs. (B4) of Ref. 11. In (59) $\hat{M}_-$ denotes the $\frac{1}{2}^+$ p-wave $KN \to KN$ amplitude (isospin T), a function of s, continued to $s - i0$. The phase-space factor is

$$\rho = Mp/16\pi^3 W , \tag{60}$$

where p refers to the nucleon momentum in the KN s channel.

A convenient multiplicative procedure[16] may be used to incorporate the two-body cut in s. A product form for $G_i(s s_i)$ is adopted:

$$G_i = \bar{G}_i F_i , \tag{61}$$

where $\bar{G}_i(s)$ contains the s cut of Eq. (59) and F_i remains to be determined. It follows from (59) that

$$\mathrm{disc}_s \bar{G}_i = 2\pi i \rho \bar{G}_i \hat{M}_- . \tag{62}$$

Because $\bar{G}_i$ depends only on s it is suitable to satisfy (62) by

$$\bar{G}_i(s) = c_i \hat{M}(s) , \tag{63}$$

in which c_i is an unknown constant; clearly (63) is consistent with the unitarity relation for $\hat{M}$:

$$\mathrm{disc}\,\hat{M} = 2\pi i \rho \hat{M} \hat{M}_- . \tag{64}$$

It is, of course, not surprising that $\bar{G}_i$ should contain an unknown constant factor in view of the role of $\bar{G}_i$ as a sort of subtraction constant in Eq. (51). Equations (61) and (63) may now be combined, absorbing the unknown c_i into F_i to write

$$G_i = \hat{M}(s) f_i . \tag{65}$$

The functions f_i must be determined such that the integral equations (45)–(47) are satisfied. In order to satisfy (64) a simple effective range form may be used for $\hat{M}$, similar to (49) but with p-wave threshold behavior.

The foregoing construction may be folded into Eqs. (45)–(47) for the determination of the residual isobar functions $f_i^{t_i}(s_i)$ (reinstating isobar variables but suppressing total energy s and isospin T); the integral equations are

$$f_1^{t_1}(s_1) = c_1^{t_1} + \sum_{t_2} \int dz_2 K_{12}^{t_1 t_2}(s_1 z_2) f_2^{t_2}(z_2) + \sum_{t_3} \int dz_3 K_{13}^{t_1 t_3}(s_1 z_3) f_3^{t_3}(z_3) , \tag{66}$$

$$f_2^{t_2}(s_2) = c_2^{t_2} + \sum_{t_1} \int dz_1 K_{21}^{t_2 t_1}(s_2 z_1) f_1^{t_1}(z_1) + \sum_{t_3} \int dz_3 K_{23}^{t_2 t_3}(s_2 z_3) f_3^{t_3}(z_3) , \tag{67}$$

$$f_3^{t_3}(s_3) = c_3^{t_3} + \sum_{t_1} \int dz_1 K_{31}^{t_3 t_1}(s_3 z_1) f_1^{t_1}(z_1) + \sum_{t_2} \int dz_2 K_{32}^{t_3 t_2}(s_3 z_2) f_2^{t_2}(z_2) . \tag{68}$$

This system of linear equations may be expressed in a generalized matrix form as

$$f = c + Kf , \tag{69}$$

in which the matrix structure spans the three isobar channels as well as the isobar isospin and subenergy within each channel. The solution to (66)–(68) can be indicated in those terms as

$$f = (1-K)^{-1} c = c + K(1-K)^{-1} c ;$$

that is,

$$f = c + \frac{K\,\mathrm{adj}(1-K)}{\det(1-K)}\, c . \tag{70}$$

Result (70) is rather schematic. It can be put into standard Fredholm form, and it can be applied directly to a numerical procedure over a selected grid of discrete subenergy points. Such quadrature methods have been employed for the less complex 3π problem.[10]

The problem of providing a unitary analytic description for the production amplitude has been addressed. The situation considered includes the complications of isospin and spin, and is restricted to s-wave systems in the three-body state, al-

though the removal of this restriction is straightforward. Unitarity is satisfied in each of the isobar subenergy variables, and two-body unitarity is satisfied in the total energy as well. The steps leading to the formal solution of the problem can be outlined as follows:

expansion into isobars, Eqs. (13) and (27)–(29) of Ref. 11;
identification of isobar factors, Eqs. (2), and their subenergy discontinuities (A1)–(A3);
identification of kinematic factors, Eqs. (24)–(26);
expression of analyticity in terms of dispersion relations, Eqs. (36) and (51);
Pasquier inversion of the double integrations, Sec. III, leading to the single-variable integral equations (45)–(47);
incorporation of the two-body cut in s, Eq. (65);
formal solution (70) to the final linear equations (66)–(68).

The parametrization of the solution includes two collections of constants, those which parametrize the relevant two-body problems [as in (49)], and the c's which appear in (63) and in the final solution (70). Only the formal development of the problem has been treated in this paper. The practical application of this work to phenomenology will be taken up in the near future.

ACKNOWLEDGMENTS

One of the authors (J.J.B.) wishes to acknowledge the hospitality at Oxford last summer and to thank Professor R. H. Dalitz for this. The work of J.J.B. is supported in part by the National Science Foundation.

APPENDIX A: THE GENERAL DISCONTINUITY FORMULAS

An important error has been spotted in Ref. 11. It occurs at the point of insertion of the isobar expansion into the discontinuity relation [Eq. (30) of that paper]. A phase factor has been overlooked in the matchup of angular coordinates necessary to unravel certain of the recoupling terms. In Eq. (30) the factor $e^{i\pi\nu''}$ should accompany the isobar amplitude $\langle m_2\mu|M_C^{Jj_2}|\lambda\rangle$. The net effect of this correction is that in all the results of Ref. 11, Sec. IV and Sec. V, the phase factor $e^{-i\pi m_2}$ should be replaced by $e^{-i\pi(m_2-\nu)}$. The correction propagates into the formulas of Appendix B, Eqs. (B5)–(B7), the corrected version of which is as follows:

$$\begin{aligned}\mathrm{disc}_1\mathfrak{M}^{J P j_1^{\hat{P}}\kappa_1} = 2\pi i\rho_1 \int d\cos\vartheta_1 \Bigg\{ &\sum_{j_2^{\pi}\kappa_2} [f_{\kappa_1\kappa_2}^{j_1^{\hat{P}} j_2^{\pi}}(\vartheta_1\vartheta_2) d^J_{\kappa_1\kappa_2}(\chi_a+\chi_b) \\ &- \eta_P\eta_\pi(-1)^{J+j_2} f_{\kappa_1-\kappa_2}^{j_1^{\hat{P}} j_2^{\pi}}(\vartheta_1\vartheta_2) d^J_{\kappa_1-\kappa_2}(\chi_a+\chi_b)] e^{-i\pi(\kappa_2-1/2)} (M^{j_2^{\pi}}\mathfrak{M}^{J P j_2^{\pi}\kappa_2})_C \\ &+ \sum_{l\xi} [f_{\kappa_1\xi}^{j_1^{\hat{P}} l+}(\vartheta_1\vartheta_3) d^J_{\kappa_1,1/2-\xi}(\chi_a) \\ &+ \eta_P(-1)^{J-1/2} f_{\kappa_1\xi}^{j_1^{\hat{P}} l-}(\vartheta_1\vartheta_3) d^J_{\kappa_1,-1/2+\xi}(\chi_a)] (M^l\mathfrak{M}^{J P l\xi})_C \Bigg\}, \end{aligned} \tag{A1}$$

$$\begin{aligned}\mathrm{disc}_2\mathfrak{M}^{J P j_2^{\hat{P}}\kappa_2} e^{-i\pi(\kappa_2-1/2)} = 2\pi i\rho_2 \int d\cos\vartheta_2 \Bigg\{ &\sum_{j_1^{\pi}\kappa_1} [f_{\kappa_2\kappa_1}^{j_2^{\hat{P}} j_1^{\pi}}(\vartheta_2\vartheta_1) d^J_{\kappa_1\kappa_2}(\chi_a+\chi_b) \\ &+ \eta_P\eta_\pi(-1)^{J+j_1} f_{\kappa_2-\kappa_1}^{j_2^{\hat{P}} j_1^{\pi}}(\vartheta_2\vartheta_1) d^J_{-\kappa_1\kappa_2}(\chi_a+\chi_b)] (M^{j_1^{\pi}}\mathfrak{M}^{J P j_1^{\pi}\kappa_1})_C \\ &+ \sum_{l\xi} [f_{\kappa_2\xi}^{j_2^{\hat{P}} l+}(\vartheta_2\vartheta_3) d^J_{1/2-\xi,\kappa_2}(\chi_b) \\ &- \eta_P(-1)^{J-1/2} f_{\kappa_2\xi}^{j_2^{\hat{P}} l-}(\vartheta_2\vartheta_3) d^J_{-1/2+\xi,\kappa_2}(\chi_b)] (M^l\mathfrak{M}^{J P l\xi})_C \Bigg\}, \end{aligned} \tag{A2}$$

$$\begin{aligned}\mathrm{disc}_3\mathfrak{M}^{J P l\xi} = 2\pi i\rho_3 \int d\cos\vartheta_3 \Bigg\{ &\sum_{j_1^{\pi}\kappa_1} [f_{\kappa_1\xi}^{j_1^{\pi} l+}(\vartheta_1\vartheta_3) d^J_{\kappa_1,1/2-\xi}(\chi_a) \\ &+ \eta_P\eta_\pi(-1)^{J+j_1} f_{-\kappa_1\xi}^{j_1^{\pi} l+}(\vartheta_1\vartheta_3) d^J_{-\kappa_1,1/2-\xi}(\chi_a)] (M^{j_1^{\pi}}\mathfrak{M}^{J P j_1^{\pi}\kappa_1})_C \Bigg\} \\ &+ \sum_{j_2^{\pi}\kappa_2} [f_{\kappa_2\xi}^{j_2^{\pi} l+}(\vartheta_2\vartheta_3) d^J_{1/2-\xi,\kappa_2}(\chi_b) - \eta_P\eta_\pi(-1)^{J+j_2} f_{-\kappa_2\xi}^{j_2^{\pi} l+}(\vartheta_2\vartheta_3) d^J_{1/2-\xi,-\kappa_2}(\chi_b)] \\ &\times e^{-i\pi(\kappa_2-1/2)} (M^{j_2^{\pi}}\mathfrak{M}^{J P j_2^{\pi}\kappa_2})_C \Bigg\} \end{aligned} \tag{A3}$$

Equation (B8) of Ref. 11 should be altered to read

$$f^{j^P_j\,\prime\,\pi}_{\kappa\kappa'}(\vartheta\vartheta') = 2\pi N_j N_{j'}[e^{j^P}_{\kappa+}(\vartheta)e^{j'^{\pi}}_{\kappa'+}(\vartheta') - e^{j^P}_{\kappa-}(\vartheta)e^{j'^{\pi}}_{\kappa'-}(\vartheta')].$$

All the other notation of Ref. 11 remains intact.

The discontinuity relations have been expressed above in terms of the isobar factors defined in Eq. (2). For the application to the isobar system described in the text, Eqs. (A1)–(A3) lead directly to Eqs. (3)–(5), the corrected version of Eqs. (85)–(87) of Ref. 11.

APPENDIX B: THE KERNEL INTEGRALS

Equations (56)–(58) contain the basic integrals involved in the explicit determination of the kernels. As one can see by relating Eqs. (41)–(43) to the assembled results of Eqs. (45)–(47), (48), and (54), the Δ_{ij} integrals are

$$\begin{aligned}
\Delta_{12} &= \Delta_{D_{12}} + \theta(-z_2)\Delta_{L_{12}},\\
\Delta_{13} &= \Delta_{D_{13}} + \theta((m-\mu)^2 - z_3)\Delta_{U_{13}} - \theta(-z_3)\Delta_{R_{13}},\\
\Delta_{21} &= \Delta_{D_{21}} + \theta(-z_1)\Delta_{L_{21}},\\
\Delta_{23} &= \Delta_{D_{23}} + \theta(-z_3)\Delta_{R_{23}},\\
\Delta_{31} &= \Delta_{D_{31}} + \theta((M-\mu)^2 - z_1)\Delta_{U_{31}} - \theta(-z_1)\Delta_{L_{31}},\\
\Delta_{32} &= \Delta_{D_{32}} + \theta((M-m)^2 - z_2)\Delta_{R_{32}} - \theta(-z_2)\Delta_{L_{32}}.
\end{aligned} \tag{B1}$$

To define the right-hand sides in (B1), let

$$\begin{aligned}
K_1 &= [(W+m)^2 - z_1]^{1/2}[(W-m)^2 - z_1]^{1/2},\\
K_2 &= [(W+\mu)^2 - z_2]^{1/2}[(W-\mu)^2 - z_2]^{1/2},\\
K_3 &= [(W+M)^2 - z_3]^{1/2}[(W-M)^2 - z_3]^{1/2},
\end{aligned} \tag{B2}$$

taking the positive branch of these and all other roots when z_i is in the decay region. Then, define

$$\Delta_{C_{ij}}(s_i z_j) = \int_{C_{ij}} \frac{dz_i}{(z_i - s_i)K_i}\,, \tag{B3}$$

where C_{ij} refers to each of the contours shown in Fig. 13 and referred to in (B1). The Γ_{ij} integrals are specified similarly to (B1), with

$$\Gamma_{C_{ij}}(s_i z_j) = \int_{C_{ij}} \frac{dz_i}{(z_i - s_i)K_i\sqrt{z_i}}\,. \tag{B4}$$

Function (B4) is an elliptic integral of the third kind. To identify it as such[17] it suffices to consider only the case of the contour D_{ij}:

$$\Gamma_{D_{ij}}(s_1 z_j) = -\frac{2}{s_1(W+m)}\,[\Pi(\phi^+_{1j}, Y_1, y_1) - \Pi(\phi^-_{1j}, Y_1, y_1)]$$

in which

$$\begin{aligned}
\sin\phi^{\pm}_{1j} &= \sqrt{z^{\pm}_{1j}}/(W-m),\\
y_1 &= (W-m)/(W+m),\\
Y_1 &= -(W-m)^2/s_1;
\end{aligned}$$

$\Gamma_{D_{2j}}(s_2 z_j)$ is similar, with $1 \to 2$ and $m \to \mu$. The notation z^+_{ij} and z^-_{ij} refers to the greater and lesser values of z_i at the end points of the contour D_{ij} for fixed z_j.

Function (B3) is of greater practical significance and should be itemized in full detail. To begin, Eqs. (B1) should be rewritten in terms of more convenient notation.[18] For Δ_{12}, Δ_{21}, and Δ_{23}:

$$\Delta_{ij} = \Delta^{(1)}_{ij} + \theta(-z_j)(\Delta^{(2)}_{ij} + \Delta^{(3)}_{ij}); \tag{B5}$$

for Δ_{13}, Δ_{31}, and Δ_{32}:

$$\Delta_{ij} = \Delta^{(1)}_{ij} + \theta(\bar{s}_{j0} - z_j)\Delta^{(2)}_{ij} + \theta(-z_j)\Delta^{(3)}_{ij}, \tag{B6}$$

in which $\bar{s}_{j0}$ refers to the pseudothreshold points $\bar{s}_{10} = (M-\mu)^2$, $\bar{s}_{20} = (M-m)^2$, and $\bar{s}_{30} = (m-\mu)^2$. It can then be shown[18] that

$$\Delta^{(1)}_{ij}(s_i z_j) = \frac{1}{K_i(s_i)} \ln \frac{E_{ij} - K_i(s_i)K_j(z_j)}{E_{ij} + K_i(s_i)K_j(z_j)}\,, \tag{B7}$$

$$\Delta^{(2)}_{ij}(s_i z_j) = \frac{1}{K_i(s_i)} \ln \frac{E'_{ij} - K_i(s_i)\,|l_j(z_j)|}{E'_{ij} + K_i(s_i)\,|l_j(z_j)|}\,, \tag{B8}$$

$$\Delta^{(3)}_{ij}(s_i z_j) = -\tfrac{1}{2}(\Delta^{(1)}_{ij} + \Delta^{(2)}_{ij}) + \frac{1}{2K_i(s_i)} \ln \frac{E_i + K_i(s_i)}{E_i - K_i(s_i)} \tag{B9}$$

in which $E_1 = s + m^2 - s_1$, $E_2 = s + \mu^2 - s_2$, and $E_3 = s + M^2 - s_3$. The quantities l_j are given by

$$\begin{aligned}
l_1 &= [z_1 - (M+\mu)^2]^{1/2}[z_1 - (M-\mu)^2]^{1/2},\\
l_2 &= [z_2 - (M+m)^2]^{1/2}[z_2 - (M-m)^2]^{1/2},\\
l_3 &= [z_3 - (m+\mu)^2]^{1/2}[z_3 - (m-\mu)^2]^{1/2}
\end{aligned} \tag{B10}$$

in the decay region, and have been continued for use in (B8). The functions $E_{ij}(s_i z_j)$ and $E'_{ij}(s_i z_j)$ are as follows:

$$\begin{aligned}
E_{12} &= -s^2 + s(s_1 + z_2 + m^2 + \mu^2) + (s_1 - m^2)(z_2 - \mu^2) - 2sM^2,\\
E_{13} &= E_{12} \quad (\text{with } z_2 \to z_3,\ M \leftrightarrow \mu),\\
E_{21} &= E_{12} \quad (\text{with } s_1 \to s_2,\ z_2 \to z_1,\ m \leftrightarrow \mu),\\
E_{23} &= E_{21} \quad (\text{with } z_1 \to z_3,\ M \leftrightarrow m),\\
E_{31} &= E_{13} \quad (\text{with } s_1 \to s_3,\ z_3 \to z_1,\ M \leftrightarrow m),\\
E_{32} &= E_{31} \quad (\text{with } z_1 \to z_2,\ m \leftrightarrow \mu),
\end{aligned} \tag{B11}$$

and

$$\begin{aligned}
E'_{1j} &= E_{1j} \quad (\text{with } s \leftrightarrow m^2,\ M \leftrightarrow \mu),\\
E'_{2j} &= E_{2j} \quad (\text{with } s \leftrightarrow \mu^2,\ M \leftrightarrow m),\\
E'_{3j} &= E_{3j} \quad (\text{with } s \leftrightarrow M^2,\ m \leftrightarrow \mu).
\end{aligned} \tag{B12}$$

APPENDIX C: THE OPE PROJECTIONS AND THE $\Delta^{(1)}$ KERNELS

The integrals $\Delta^{(1)}_{ij}$ and Γ_{ij} of Appendix B develop an imaginary part in those regions of the kinematic

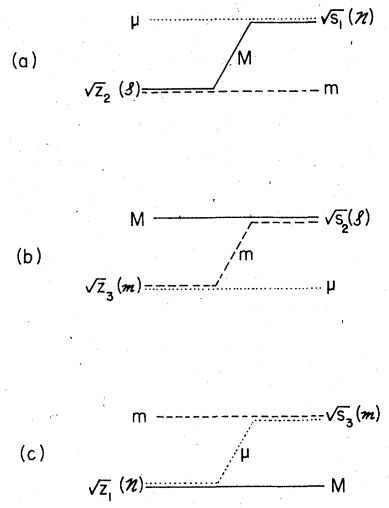

FIG. 14. One-particle-exchange processes.

(s_i, z_j) plot (analogous to Fig. 3) which correspond to possible physical processes. In the physical region, call it $\mathfrak{D}$, for the three-body production process one finds

$$\mathrm{Im}\Delta_{ij}^{(1)} = \pi/K_i \quad \text{and} \quad \mathrm{Im}\Gamma_{ij} = \pi/K_i\sqrt{s_i}$$

for $s_i, z_j \in \mathfrak{D}$. Thus in $\mathfrak{D}$, Eqs. (56)–(58) imply that

$$\mathrm{Im}I_{12} = \pi A/K_1,$$

$$\mathrm{Im}I_{23} = \pi B/K_2,$$

$$\mathrm{Im}I_{31} = \pi C/K_3,$$

where A, B, and C are obtained from the lengthy kinematical factors in (56)–(58); for example, $B = 1 + P_0(z_3) + P_{20}(s_2) + P_{b0}(s_2)$.

Consider now the Feynman graphs for the possible OPE processes between s-wave isobars, shown in Fig. 14. The isobars are denoted by: $\mathfrak{N} = (\pi N)$, $\mathfrak{S} = (KN)$, and $\mathfrak{m} = (K\pi)$. Because these are s-wave pairs their coupling vertices are simply $\bar{\mathfrak{N}}N\pi$, $\bar{\mathfrak{S}}NK$, and $\mathfrak{m}^*K\pi$. As shown in the figure the isobar legs have masses $\sqrt{s_i}$ and $\sqrt{z_j}$. The $J^P = \frac{1}{2}^+$ projections of these graphs can be computed, following the technique for partial-wave analysis of Gell-Mann *et al.*[19] If these projections are called Π_{ij}, the results (omitting common kinematic factors) are

(a) $\Pi_{12} = -sM[(s_1 z_2)]^{1/2} A\Delta_{12}^{(1)}/K_2 + \frac{1}{2}(M + W + \sqrt{s_1} + \sqrt{z_2})$,

(b) $\Pi_{23} = -sM\sqrt{s_2} B\Delta_{23}^{(1)}/K_3 - \frac{1}{2}$,

(c) $\Pi_{31} = -sM\sqrt{z_1} C\Delta_{31}^{(1)}/K_1 - \frac{1}{2}$,

corresponding to Figs. 14(a)–14(c). It follows that the imaginary part of Π_{ij} in $\mathfrak{D}$ is proportional to that of the kernel I_{ij}.

Further, if the substitution $\Gamma_{ij} \to \Delta_{ij}/\sqrt{s_i}$ is made, then only Δ_{ij} occurs in I_{ij}; one finds from Eqs. (56)–(58) that

$$I_{12} \to A\Delta_{12},$$

$$I_{23} \to B\Delta_{23},$$

$$I_{31} \to C\Delta_{31}.$$

Thus the $\Delta_{ij}^{(1)}$ part of I_{ij} is very simply related to the corresponding Π_{ij}, so that, for those parts of the kernels which cover the physical region $\mathfrak{D}$, a physical interpretation in terms of one-particle-exchange has been established.

[1] E.g., L. F. Cook and B. W. Lee, Phys. Rev. 127, 283 (1962).

[2] E.g., M. G. Olsson and G. B. Yodh, Phys. Rev. 145, 1309 (1966).

[3] E.g., D. J. Herndon, P. Söding, and R. J. Cashmore, Phys. Rev. D 11, 3165 (1975).

[4] E.g., D. J. Herndon *et al.*, Phys. Rev. D 11, 3183 (1975).

[5] R. Aaron and R. D. Amado, Phys. Rev. D 13, 2581 (1976).

[6] I. J. R. Aitchison and R. J. A. Golding, Phys. Lett. 59B, 288 (1975).

[7] I. J. R. Aitchison, Phys. Rev. 137, B1070 (1965).

[8] R. D. Amado, Phys. Rev. Lett. 33, 333 (1974).

[9] I. J. R. Aitchison, J. Phys. G 3, 121 (1977).

[10] I. J. R. Aitchison and R. J. A. Golding, J. Phys. G 4, 43 (1978).

[11] J. J. Brehm, Ann. Phys. 108, 454 (1977).

[12] Y. Goradia and T. A. Lasinski, Phys. Rev. D 15, 220 (1977).

[13] R. Pasquier and J. Y. Pasquier, Phys. Rev. 170, 1294 (1968).

[14] T. W. B. Kibble, Phys. Rev. 117, 1159 (1960).

[15] C. Kacser, J. Math. Phys. 7, 2008 (1966).

[16] J. J. Brehm, Phys. Rev. D 15, 776 (1977).

[17] W. Gröbner and N. Hofreiter, *Integraltafel* (Springer, New York, 1965), pp. 59 and 78ff.

[18] I. J. R. Aitchison and C. Kacser, Nuovo Cimento 40, 576 (1965).

[19] M. Gell-Mann, M. L. Goldberger, F. E. Low, E. Marx, and F. Zachariasen, Phys. Rev. 133, B145 (1964).